Novel electroabsorption modulator monolithically integrated with spot-size converter

Lianping Hou (侯廉平), Wei Wang (王 圩), and Hongliang Zhu (朱洪亮)

National Research Center for Optoelectronic Technology, Institute of Semiconductors, Chinese Academy of Sciences, Beijing 100083

Received August 18, 2004

A novel 1.55-μm spot-size converter integrated electroabsorption modulator was designed with conventional photolithography and chemical wet etching process. A ridge double-core structure was employed for the modulator, and a buried ridge double-core structure was incorporated for the spot-size converter. The passive waveguide was optically combined with a laterally tapered active waveguide to control the mode size. The figure of merit is 4.1667 dB/V(/100 μm) and the beam divergence angles in the horizontal and vertical directions were as small as 11.2° and 13.0°, respectively.

OCIS codes: 250.7360, 350.5500, 230.3120.

In recent years, the electroabsorption modulator (EAM) is attractive as an external modulator because of its advantages such as low power consumption, low drive voltage, small size, large bandwidth, polarization intensitivity, and potential for monolithic integration with other components[1−3]. An optical device integrated with a spot-size converter (SSC) has been paid more attention for its direct coupling to an optical fiber with low loss, large alignment tolerances, and simple packaging schemes without using a micro-lens or tapered fiber[4]. EAM integrated with a SSC (EAM-SSC) is much more attractive for low-cost packaging due to its large spot size which is well matched to that of a single-mode fiber (SMF)[5−9].

To achieve low-loss, alignment-tolerant coupling, the small elliptical beam from the EAM has to be mode-matched to the larger, circular beam in the fiber. So far, there is mainly three classes of SSC that have been developed to expand the laser optical mode. The first one is the vertical SSC in which the waveguide thickness decreases along the output direction[10]. In the second one, the active region is laterally tapered, which is formed by decreasing the waveguide width[11]. The third one is so-called double-core taper in which the active waveguide is laterally tapered and combined with an underlying passive waveguide[12]. So far, most of them were based on buried structure with or without selective area growth[3,5,6]. Moreover, most of them involve complex growth steps, excessive processing steps, strict process tolerance, and poor device performance. In this letter, a novel 1.55-μm EAM-SSC was fabricated by simple process in which the active waveguide is laterally tapered and combined with an underlying passive waveguide. The taper shape and the passive waveguide can be optimized independently, which allows to easily control the beam divergence at the output facet[13]. For the EAM, a ridge double-core structure is employed. For the spot-size converter, a buried ridge double-core structure (BRS) is incorporated. The combination of ridge and BRS structure can take advantages of both easy processing of ridge structure and the excellent mode characteristic of BRS. This is the first time that such structure is reported as far as we know. Furthermore, the novel EAM-SSC was easily fabricated using only two-step low-pressure metal-organic vapor phase epitaxy (LP-MOVPE) growth.

The schematic layout of the device is shown in Fig. 1. The device consists of three sections, namely the untapered part of the active region (EAM section), the tapered section and the passive secondary guide, which are used to expand and stabilize the beam for efficient coupling to a SMF. The active section of modulator can be optimized independently to meet the requirements such as total insertion loss, extinction ration (ER), modulation rate, drive voltage, chirp parameter, and so on. The tapered section is designed to butt-couple most of the optical power and to perform low-loss adiabatic mode expansion. The passive secondary guide is designed to stabilize and optimize the near field pattern to match that of a cleaved SMF.

The variations of transverse spot sizes with the fabrication parameters, for both the tapered primary and passive secondary isolated guides and also when they are coupled together to form a structure, are studied by three-dimensional (3D) beam propagation method (BPM) analysis. Figure 2(a) shows the effective index (β/k_0) and the transverse spot size versus the active waveguide width, in which the active thickness is kept constant at 0.275 μm. In this work, the full width of spot size is defined as the distance between two points, where the light amplitued is $1/e$ of its

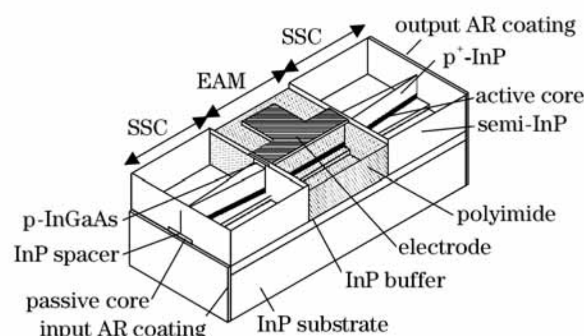

Fig. 1. Schematic of the EAM-SSC. AR: anti-reflection.

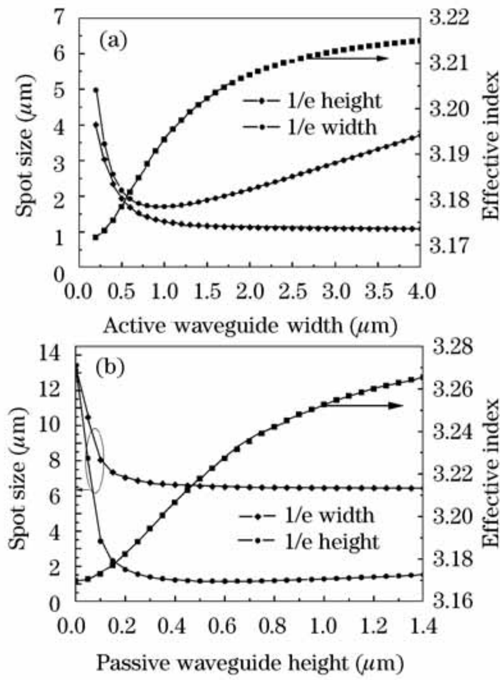

Fig. 2. Transverse spot sizes and effective index versus the active core width (a) and passive core thickness (b).

maximum value (or the power intensity is $1/e^2$). Figure 2(b) shows the transverse spot sizes versus the passive waveguide thickness, in this case, the waveguide width is fixed at 8 μm.

As shown in Fig. 2, the lateral spot size is primarily related to the width of waveguide and nearly constant until the mode cutoff is obtained, the vertical spot size is predominantly controlled by the core thickness. Decreasing the stripe width from 4 to 0.5 μm does not increase the mode size, for stripe widths below 0.5 μm, the mode size increases rapidly. Similarly, decreasing the passive core thickness from 1.4 to 0.2 μm does not increase the mode size, and for passive core thickness below 0.2 μm, the mode size increases rapidly. This may be varied to achieve a large spot size, similar to that of a SMF. When the core thickness is 50 nm, the mode profile is nearly circular, as both $1/e$ width and $1/e$ height are almost equal.

In order to have a nearly adiabatic tapering behavior, i.e., a minimal loss, a longer and nonlinear taper shape SSC is necessary. This is because rapid decrease of the taper width along the beam propagation axis can not efficiently expand the propagating field.

Polarization dependence of electroabsorption multi quantum well (MQW) material has been studied extensively. The polarization dependence is a result of a number of factors including the waveguide geometry, the optical selection rule, the transition strength, and the nature of electroabsorption effect.

The extinction ratio, defined as the on-state and off-state power transmission ratio is calculated from

$$ER = 4.343 \cdot \Gamma \cdot [\alpha_{\mathrm{QW}}(V_{\mathrm{off}}) - \alpha_{\mathrm{QW}}(V_{\mathrm{on}})] \cdot L, \tag{1}$$

where Γ is the optical confinement factor (OFC) defined as the ratio of optical power in the EAM waveguide (the MQW and separated confined heterostructure (SCH) region) and the total power in all propagation space, it can be calculated from

$$\Gamma = \frac{\iint\limits_{\mathrm{WG}} |U_{\mathrm{WG}}|^2 \,\mathrm{d}x\mathrm{d}y}{\iint\limits_{\text{all space}} |U_{\mathrm{WG}}|^2 \,\mathrm{d}x\mathrm{d}y}, \tag{2}$$

$\alpha_{\mathrm{QW}}(V_{\mathrm{on}})$ and $\alpha_{\mathrm{QW}}(V_{\mathrm{off}})$ are the quantum well absorption coefficient in on-state and off-state individually, which is dependent on applied voltage and incident light energy. Roughly, the heavy- and light-hole bandgap should be identical in order to achieve the same absorption coefficient α_{QW}. This is obviously not the case when holes are confined in unstrained quantum wells since the quantum confinement energy depends on the carrier effective mass, which results in narrow bandgap for heavy-hole transition in InGaAsP quantum wells. By carefully adjusting layer composition, tensile strain, and quantum-well width, the transition energies related to heavy and light holes were matched, yielding polarization independent modulation performance.

While the higher number of quantum wells increases the overlap between the applied electric field and optical field, it reduces the electric field strength across the active region. Hence, an optimization for well numbers and width and the EAM length is necessary to maximize the electroabsorption efficiency of the modulator. A design trade-off is also necessary between high electroabsorption efficiency and high bandwidth, since a thicker guiding layer reduces the capacitance and therefore increases the modulation bandwidth. The simulation has shown that the optimum well width is $8-10$ nm to achieve the highest ER[14].

The p-cladding thickness is an important parameter in waveguide design because if this layer is too thin, the cap layer (lattice matched InGaAs has an absorption wavelength of 1.67 μm) causes large optical loss, while a too thick cap layer causes deeper zinc diffusion into the intrinsic region. In order to avoid excess absorption of the contact layer, the cladding layer thickness should be greater than 1.8 μm, otherwise some of light enters the contact layer and cannot be modulated, consequentially the ER becomes small. For the same reason, the InGaAs contact layers in the two SSC segments should be removed.

According to above analysis, the EAM-SSC was constructed in double-core structure: the EAM active waveguide was in a ridge double-core and the SSC in a buried double-core shape. The lengths of EAM and SSC were both 200 μm. The active waveguide was formed in three parts: a straight active region (EAM section) in which the active waveguide was 2 μm wide and two regions (SSC section) in which the width were linearly tapered from 2 μm to 0. Since the passive waveguide was 8 μm wide and sufficiently thin, most of the optical power was confined in the active waveguide in the EAM section. However, in the SSC sections, the optical power was gradually transferred to the passive waveguide as the width of the active waveguide became narrow. Eventually, at the mirror facet, the optical mode was determined only by the thin passive waveguide.

Compared with previously reported double-core SSC, our structure does not rely on multilayer

waveguides[15,16], so that growth was easier and conventional chemical wet etching could be performed straightforwardly using the guiding layer as a stop etch.

The EAM-SSC was fabricated by only two steps of MOVPE growth. The n-doped InP buffer, 50-nm-thick passive guiding layer (InGaAsP, $\lambda = 1.125\mu$m), 0.2-μm InP spacer, the active layer and p-doped InP (1.8 μm), and contact layers (0.2 μm) were grown successively. The active layer included a tensile strained (-0.3%)-MQW active layer consisting of eight wells (well/barrier = 10 nm/5 nm, $\sim$115 nm thick) for 1.50-μm peak photoluminescence wavelength, SCH layers (80 nm, $\lambda = 1.125$ μm) on both sides of the MQW-layer.

During the active and passive waveguide mesa formation, chemical wet etching method was used. A sharp taper tip less than 0.2 μm at SSC section was easily achieved by normal photolithography combined with an undercut etching. So, there is no need for a submicron patterning using expensive and time-consuming e-beam lithography. Before the mesa formation, the InGaAs contact layer in SSC segment was removed by "311" etchant ($3H_2SO_4$:$1H_2O_2$:$1H_2O$). After mesa etching, the electroabsorption segment was masked by SiO_2, and then the two SSC segments are buried by 2.5-μm-thick semi-InP. Passivation and electrical isolation of the ridge sidewalls was accomplished through a 250-nm-thick plasma enhanced chemical vapor deposition (PECVD) grown SiO_2 layer.

Polyimide was used for planarization deep ridge EAM structure and reduces its spurious capacitance to enhance the modulation bandwidth. After a contact hole etched on top of the ridges, standard p- and n-metal layers were evaporated. In order to reduce the end face reflection and the insertion loss, both sides of mirrors were deposited with AR coatings.

Figure 3 shows the device capacitance versus the reverse voltage which was measured at 1-MHz frequency. A bond pad metallization on top of a 2.4-μm-thick polyimide layer results in 0.14-pF parasitic capacitance. The intrinsic layer of the PIN junction was 0.36-pF at a -2-V bias. The total device capacitance is 0.5 pF at a reverse bias of 2 V which leads to 12-GHz bandwidth.

Figure 4 shows the DC extinction ratio curves of the modulator in which the incident light wavelength is 1550 nm. High extinction ratio of 25 dB was achieved at a reverse bias of 3 V. The figure of merit is 4.1667 dB/V(/100 μm). The dependence of polarization sensitivity observed in ER in the wavelength range of $1530 -$ 1570 nm is below 1.3 dB even at high extinction ratio larger than 10 dB.

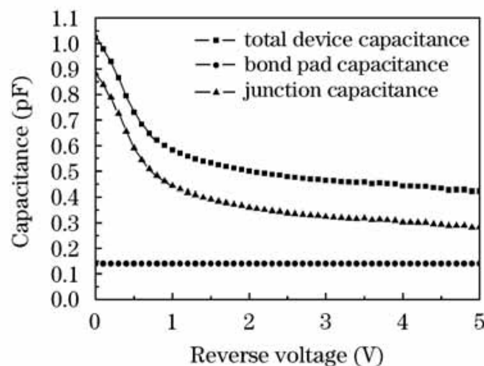

Fig. 3. The device capacitance versus the reverse voltage.

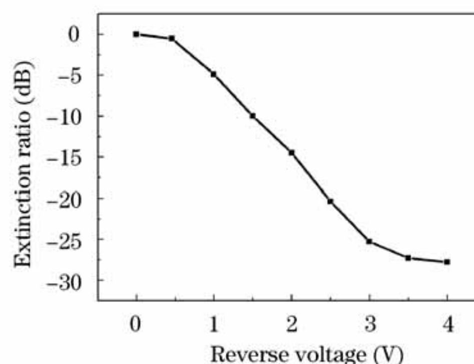

Fig. 4. The DC extinction ratio curves of modulator at 1550-nm wavelength.

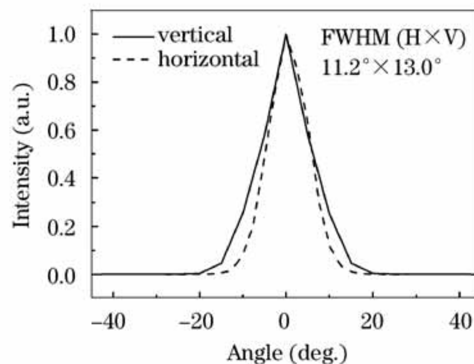

Fig. 5. Far-field pattern from the SSC facet. FWHM: full-width at half-maximum.

Figure 5 shows the far field pattern observed from SSC facet. Its divergence angles are as small as 11.2° (horizontal)$\times$13.0° (vertical), corresponding to the output field mode size of 6.0 μm (horizontal) $\times$4.8 μm (vertical). On the other hand, those from the EAM facet are 37.63° and 36.35°, corresponding to the output field mode size of 1.74 μm (horizontal) $\times$ 1.1 μm (vertical). When coupled to a cleaved SMF, coupling loss and -1-dB align tolerance for EAM-SSC was about 3 dB, ($\pm$ 2.9 μm)$\times$($\pm$ 2.56 μm) for horizontal and vertical directions, respectively. However, those without SSC were about 10 dB, ($\pm$ 1.9 μm)$\times$($\pm$ 1.6 μm).

In summary, a novel 1.55-μm EAM-SSC with bandwidth exceeding 10 GHz was optimized designed and easily fabricated. The figure of merit was 4.1667 dB/V(/100 μm) and the beam divergence angles in the horizontal and vertical directions were as small as 11.2° and 13.0°, respectively. Simple fabrication procedure and high performance of the device prove that it would be suitable for low cost and mass-production external modulators for 10-GHz optical access network.

This work was supported by the National Natural Sciences Foundation of China (No. 90101023) and the National "973" Project of China (No. 20000683-1). L. Hou's e-mail address is houlp@red.semi.ac.cn.

References

1. F. Devaux, F. Dorgeuille, A. Ougazzaden, F. Huet, M. Carré, A. Carenco, M. Henry, Y. Sorel, J.-F. Kerdiles, and E. Jeaney, IEEE Photon. Technol. Lett. **5,** 1288 (1993).
2. T. Ido, H. Sato, D. J. Moss, S. Tanaka, and A. Takai, IEEE Photon. Technol. Lett. **6,** 1207 (1994).
3. F. Devaux, P. Bordes, A. Ougazzaden, M. Carré, and F. Huet, Electron. Lett. **30,** 1347 (1994).
4. A. Lestra and J.-Y. Emery, IEEE J. Sel. Top. Quantum Electron. **3,** 1429 (1997).
5. U. Koren, B. I. Miller, M. G. Young, M. Chien, G. Raybon, T. Brenner, R. Ben-Michael, K. Dreyer, and R. J. Capik, Electron. Lett. **32,** 111 (1996).
6. J. E. Johnson, L. J.-P. Ketelsen, J. A. Grenko, S. K. Sputz, J. Vandenberg, M. W. Focht, D. V. Stampone, L. J. Peticolas, L. E. Smith, K. G. Glogovsky, G. J. Przybylek, S. N. G. Chu, J. L. Lentz, N. N. Tzafara, L. C. Luther, T. L. Pernell, F. S. Walters, D. M. Romero, J. M. Freund, C. L. Reynolds, L. A. Gruezke, R. People, and M. A. Alam, IEEE J. Sel. Top. Quantum Electron. **6,** 19 (2000).
7. W.-J. Choi, A. E. Bond, J. Kim, J. Zhang, R. Jambunathan, H. Foulk, S. O'Brien, J. Van Norman, D. Vandegrift, C. Wanamaker, J. Shakespeare, and H. Cao, J. Lightwave Technol. **20,** 2052 (2002).
8. B. Mason, A. Ougazzaden, C. W. Lentz, K. G. Glogovsky, C. L. Reynolds, G. J. Przybylek, R. E. Leibenguth, T. L. Kercher, J. W. Boardman, M. T. Rader, J. M. Geary, F. S. Walters, L. J. Peticolas, J. M. Freund, S. N. G. Chu, A. Sirenko, R. J. Jurchenko, M. S. Hybertsen, L. J. P. Ketelsen, and G. Raybon, IEEE Photon. Technol. Lett. **14,** 27 (2002).
9. K. Asaka, Y. Suzaki, Y. Kawaguchi, S. Kondo, Y. Noguchi, H. Okamoto, R. Iga, and S. Oku, IEEE Photon. Technol. Lett. **15,** 679 (2003).
10. O. Mitomi, N. Yoshimoto, K. Magari, T. Ito, Y. Kawaguchi, Y. Suzaki, Y. Tohmori, and K. Kasaya, J. Lightwave Technology. **17,** 1255 (1999).
11. P. Doussiere, P. Garabedian, C. Graver, D. Bonnevie, T. Fillion, E. Derouin, M. Monnot, J. G. Provost, D. Leclerc, and M. Klenk, IEEE Photon. Technol. Lett. **6,** 170 (1994).
12. R. Y. Fang, D. Bertone, M. Meliga, I. Montrosset, G. Oliveti, and R. Paoletti, IEEE Photon. Technol. Lett. **9,** 1084 (1997).
13. I. F. Lealman, L. J. Rivers, M. J. Harlow, S. D. Perrin, and M. J. Robertson, Electron. Lett. **30,** 857 (1994).
14. S. Nojima and K. Wakita, Appl. Phys. Lett. **53,** 1958 (1988).
15. V. Vusirikala, S. S. Saini, R. E. Bartolo, R. Whaley, S. Agarwala, M. Dagenais, F. G. Johnson, and D. Stone, IEEE Photon. Technol. Lett. **9,** 1472 (1997).
16. H. Sato, M. Aoki, M. Takahashi, M. Komori, K. Uomi, and S. Tsuji, Electron. Lett. **31,** 1241 (1995).